Studies of Polaritonic States for a 2D Hénon-Heiles System

Alexandre Menard (L3-Mag1 Fundamental Physics)
supervised by Pascal Parneix
within the SYSTEMAE team

June 10 - July 19, 2024

Institute of Molecular Sciences of Orsay - UMR 8214
André Rivière Street - Building 520
91405 Orsay Cedex

Abstract

The static and dynamic evolution of vibrational states coupled to a Fabry-Perot micro-cavity's electromagnetic mode is studied under a Hénon-Heiles potential to model the reactivity of a linear triatomic molecule. After introducing a change from normal coordinates to oblique ones, the Pauli-Fierz Hamiltonian describing light-matter interaction is discussed. Various resolution approximations are introduced, and a convergence study is proposed for subsequent simulations. The appearance of a Fermi resonance in static simulations with added anharmonicity to the Hénon-Heiles potential highlights the importance of this potential surface structure on the system's ability to exhibit experimentally observed behaviors. Polaritonic states involved in the Fermi doublet are dynamically studied by preparing two molecules in each state before inserting them into the cavity. Vibrational energy redistributions are observed in each case, along with photon absorptions-emissions during vibrational exchanges. Lastly, the previously discussed model is extended to a system of N molecules, with constraints on total energy, cumulative excitations, and polaritons for individual systems proposed. These constraints aim to significantly reduce the eigenvalue problem size to speed up model analysis iterations and enable study with a higher number of molecules. The upper limit of the number of molecules, N, remains the same order of magnitude, with exponential complexity still present due to the problem's nature.

Acknowledgments

It is impossible for me to begin without thanking my internship supervisor, Mr. Pascal Parneix, for proposing this internship subject and for supervising me during these six weeks. This internship was my first interaction with university research, and for that, I am grateful and thank him for all his patience, explanations, kindness, confidence and everything this internship brought me, starting from discovering his research subject, to numerical methods, and for everything that will follow in this report.

I also thank Elena Magdalena Staicu-Casagrande and Hocine Khemliche for the few exchanges we had, but also for accepting that a close friend visit their experimental GIFAD (Grazing Incident Fast Atom Diffraction) setup, as well as all the explanations about the manipulation and femtosecond lasers.

I thank the doctoral student Christian Perest Sonny Tsotezem in the Nanophysics and surfaces team for our passionate discussions, the few pieces of advice for my future studies and for sharing the difficulties encountered as a doctoral student which will be valuable experience feedback for the future.

I thank the entire team of the Institute of Molecular Sciences of Orsay (ISMO) for their warm and welcoming reception.

Finally, it is important for me to thank all the contributors, often forgotten and neglected for their contributions, whatever the nature of their contributions, in open-source projects related directly or indirectly to Fortran, Python and their libraries. Without these contributors, this work could not have come to light. For this reason, these tools are referenced in the bibliography and deserve fair recognition for the contributions these tools brought to this report.

Contents

Introduction

Polaritonic states are hybrid states between light and matter where molecular vibrational excitations are strongly coupled to the electromagnetic field within a micro-cavity. The molecule-cavity coupling is mainly of dipolar nature and will therefore be linked to the molecule's dipole and the vacuum electric field E_0, proportional to $1/\sqrt{V_c}$, V_c being the microcavity volume. These states have generated strong interest in recent years in the molecular sciences community, particularly for demonstrating the modification of reactivity of molecules coupled to a cavity [1], [2]. Although current knowledge cannot experimentally control reactivity, understanding the processes on a theoretical level is an essential challenge for producing experiments capable of opening and choosing new reactive pathways.

These states have been studied for one-dimensional potentials, both symmetric and asymmetric ([2]), and more recently on two-dimensional potentials like the Hénon-Heiles potential ([3], [4], [5]) which will be the subject of this report. The Hénon-Heiles potential, under certain conditions, presents two oscillation modes like for a linear triatomic molecule of cyanide type ($\mathrm{HC} \equiv \mathrm{N}$). The Hénon-Heiles system therefore presents two vibrational frequencies $\omega_{\min}$ and $\omega_{\max}$. In the case where $\omega_{\max} \approx 2\omega_{\min}$, a Fermi resonance can appear due to the anharmonicity of the potential.

Within the SYSTEMAE team of the Institute of Molecular Sciences of Orsay (ISMO), P. Parneix is interested in two potential models. The first model is a case of resonance between the cavity frequency and the second vibrational mode $\omega_{\min}$ in a situation that does not present a Fermi resonance. This leads to avoided crossings around which vibrational energy is redistributed in the molecule between different modes. The second model is studied with the first vibrational mode $\omega_{\min}$ in resonance with the cavity. In this case, a Fermi resonance (or a Fermi doublet) can be observed, which will be the purpose of this work.

This report is therefore part of his work on polaritons, where a study of the second model will be carried out for different values of inter-mode anharmonic coupling.

The second part of this report will propose an extension of the model to a system of N molecules, starting with the theoretical framework with all inter-molecular interactions.

1. Theory of Polaritonic States

1.1. Study of the Hénon-Heiles Potential Surface

The two-dimensional Hénon-Heiles (HH) potential $V(q_1, q_2)$ is written in normal coordinates:

$$V(q_1, q_2) = \frac{1}{2}k_{11}q_1^2 + \frac{1}{2}k_{22}q_2^2 + k_{112}q_1^2q_2 + k_{222}q_2^3 \tag{1}$$

where the k_{ii}, k_{ii2} are force constants determining the characteristics of the potential energy surface (PES). The properties of this surface are governed by the dimensionless parameters $\kappa = \frac{k_{222}}{k_{112}}$ and $\eta = \frac{2k_{22}}{3k_{11}}$. In this work, the parameters of $V(q_1, q_2)$ are chosen such that $0 < \kappa < \eta$. In this configuration, the PES has two saddle points S_1, S_2 of the same energy, a maximum A and a local minimum at the origin O (see figure 3 in section 1.5.). This potential can then be interpreted as a model of a linear triatomic molecule of the HC ≡ N type presenting two coupled stretching modes and two equivalent dissociation pathways (via the path $O \to S_1/S_2 \to -\infty$).

1.2. Hamiltonian of the Hénon-Heiles Potential

$$H_{\text{HH}}(q_1, q_2) = \sum_{i=1}^{2}\left(-\frac{1}{2\mu_i}\frac{\partial^2}{\partial q_i^2}\right) + V(q_1, q_2), \quad \omega_i = \sqrt{\frac{k_{ii}}{\mu_i}} \tag{2}$$

The coupled and anharmonic nature of the potential does not allow analytical determination of the eigenstates of this Hamiltonian (2). It has been shown by Zúñiga et al.'s team [4] that numerical convergence of bound state energies is faster using a set of oblique coordinates. The coordinate change is summarized below and begins with a +45° orthogonal rotation:

$$\begin{cases} R = \left(\frac{\mu_1}{\mu_2}\right)^{\frac{1}{4}} \\ r_1 = \frac{1}{\sqrt{2}}\left(Rq_1 + \frac{q_2}{R}\right) \\ r_2 = \frac{1}{\sqrt{2}}\left(\frac{q_2}{R} - Rq_1\right) \end{cases} \xrightarrow[\text{parameters}]{\text{model}} \begin{cases} \mu' &= \sqrt{\mu_1\mu_2} \\ k'_{11} &= k'_{22} = \frac{\mu'}{2}(\omega_1^2 + \omega_2^2) \\ k'_{12} &= \frac{\mu'}{2}(\omega_2^2 - \omega_1^2) \\ k'_{111} = k'_{222} &= \frac{1}{2\sqrt{2}}\left(\frac{k_{112}}{R} + R^3k_{222}\right) \\ k'_{112} = k'_{122} &= \frac{1}{2\sqrt{2}}\left(3R^3k_{222} - \frac{k_{112}}{R}\right) \end{cases} \tag{3}$$

The Hamiltonian in the new coordinate set (r_1, r_2) becomes:

$$H_{\text{HH}}(r_1, r_2) = \sum_{i=1}^{2}\left(-\frac{1}{2\mu'}\frac{\partial^2}{\partial r_i^2} + \frac{1}{2}k'_{ii}r_i^2 + k'_{iii}r_i^3\right) + k'_{12}r_1r_2 + k'_{112}r_1^2r_2 + k'_{122}r_1r_2^2 \tag{4}$$

A final non-orthogonal transformation, parameterized by $|a| < 1$, is performed according to:

$$\begin{cases} o_1 = \frac{1}{(1-a^2)^{\frac{1}{2}}}(r_1 + ar_2) \\ o_2 = \frac{1}{(1-a^2)^{\frac{1}{2}}}(ar_1 + r_2) \end{cases} \xrightarrow[\text{parameters}]{\text{model}} \begin{cases} \mu &= \frac{1-a^2}{1+a^2}\mu' \\ \mu_{12} &= \frac{1-a^2}{2a}\mu' \\ U_{11} = U_{22} &= \mu'\left(\frac{k'_{12}}{\mu} - \frac{k'_{11}}{\mu_{12}}\right) \\ U_{111} = U_{222} &= \frac{(1-a)[(1+a+a^2)k'_{111} - ak'_{112}]}{(1-a^2)^{\frac{3}{2}}} \\ U_{112} = U_{122} &= \frac{(1-a)[(1-a+a^2)k'_{112} - 3ak'_{111}]}{(1-a^2)^{\frac{3}{2}}} \end{cases} \tag{5}$$

The Hamiltonian in oblique coordinates is then given by:

$$
\begin{aligned}
H_{\mathrm{HH}}(o_1,o_2) = \sum_{i=1}^{2} h_i(o_i) \qquad & h_i(o_i) = \left(-\frac{1}{2\mu}\frac{\partial^2}{\partial o_i^2} + \frac{1}{2}U_{ii}o_i^2 + U_{iii}o_i^3 \right) \\
+V_2(o_1,o_2) \qquad & V_2(o_1,o_2) = -\frac{1}{\mu_{12}}\frac{\partial^2}{\partial o_1 \partial o_2} + U_{12}o_1o_2 \\
+V_3(o_1,o_2) \qquad & V_3(o_1,o_2) = U_{112}o_1^2o_2 + U_{122}o_1o_2^2
\end{aligned}
\tag{6}
$$

The parameter a, introduced in the oblique transformation, is chosen to eliminate coupling between polyads[1] $\nu_1+\nu_2 \leftrightarrow \nu_1+\nu_2 \pm 2$:

$$
\langle \nu_1,\nu_2|V_2|\nu_1 \pm 1, \nu_2 \pm 1\rangle = 0 \tag{7}
$$

where $|\nu_1,\nu_2\rangle$ are the eigenvectors of two uncoupled quantum harmonic oscillators.

This condition (7) was proposed by Zúñiga et al.'s team [4], and is satisfied for $a = \tan(\alpha_0)$ where $\sin(2\alpha_0) = \frac{\omega_2-\omega_1}{\omega_1+\omega_2}$, the angle α_0 corresponding to the opening (or closing depending on the potential energy surface parameters) angle of the axes (o_1,o_2) with respect to (r_1,r_2).

The DVR method [6] is used to obtain the eigenstates $\left\{\left|n_k^i\right\rangle\right\}$ with eigenvalues $\omega_{n_k^i}$ of the Hamiltonian $h_i(o_i)$. Note that $\left|n_k^1\right\rangle = \left|n_k^2\right\rangle$ and $\omega_{n_k^1} = \omega_{n_k^2}$ since $h_1 = h_2$. This basis will then be used to determine the eigenstates of the total Hamiltonian from a variational approach.

1.3. Pauli-Fierz Hamiltonian: light-matter coupling

The isolated HH system is assumed coupled to a single mode ω_c of the electromagnetic field with amplitude E_0 in a cavity. The coupling intensity will be characterized by the dimensionless parameter λ_c. The system evolution is then described by the Pauli-Fierz Hamiltonian H_{PF}. We denote n_p the number of photons in the cavity with $\left|n_p\right\rangle$ the Fock states, n_i the number of excitations according to the vibrational mode along axis o_i, and $|\boldsymbol{n}\rangle = |n_1,n_2\rangle$. We finally define the electric dipole operator $\hat{d}$ where d_{ij} is the matrix element between the i-th excited state and the j-th excited state of the isolated HH system. The total Hamiltonian is written in Dirac notation as:

$$
\begin{aligned}
H_{\mathrm{PF}} = & \sum_{n_p,\boldsymbol{n}} \left(n_p\omega_c + \omega_{n_1} + \omega_{n_2}\right)\left|n_p,\boldsymbol{n}\right\rangle\left\langle n_p,\boldsymbol{n}\right| + \sum_{n_p,\boldsymbol{n},\boldsymbol{n}'} \langle \boldsymbol{n}|(V_2+V_3)|\boldsymbol{n}'\rangle \left|n_p,\boldsymbol{n}\right\rangle\left\langle n_p,\boldsymbol{n}'\right| \\
& + \lambda_c\omega_c \sum_{n_p,\boldsymbol{n},\boldsymbol{n}'} \frac{\left\langle \boldsymbol{n}\middle|\hat{d}\middle|\boldsymbol{n}'\right\rangle}{d_{01}} \left(\left|n_p,\boldsymbol{n}\right\rangle\left\langle n_p+1,\boldsymbol{n}'\right| + \left|n_p+1,\boldsymbol{n}\right\rangle\left\langle n_p,\boldsymbol{n}'\right|\right) \\
& + \lambda_c^2\omega_c \sum_{n_p,\boldsymbol{n},\boldsymbol{n}'} \frac{\left\langle \boldsymbol{n}\middle|\hat{d}^2\middle|\boldsymbol{n}'\right\rangle}{d_{01}^2} \left|n_p,\boldsymbol{n}\right\rangle\left\langle n_p,\boldsymbol{n}'\right|
\end{aligned}
\tag{8}
$$

where we set $\lambda_c = \frac{E_0 d_{01}}{\omega_c}$, $\omega_c = \omega_{10}(1+\Delta)$ with $|\Delta| \ll 1$, a parameter allowing control of the cavity frequency deviation from the first excited level ω_{10} of the HH system (the ground state energy being chosen as zero).

A priori, the Hamiltonian H_{PF} develops on an infinite-dimensional space $\mathcal{H} = \left\{\left|n_p,n_1,n_2\right\rangle, \left(n_p,n_1,n_2\right) \in \mathbb{N}^3\right\}$. Since exact resolution is not possible, numerical resolution is performed in a finite subspace $\mathcal{H}' = \left\{\left|n_p,n_1,n_2\right\rangle, \left(n_p,n_1,n_2\right) \in [\![0,N_p-1]\!] \times [\![0,N_{\max}-1]\!]^2\right\}$, with

[1] For eigenstates $|\nu_1,\nu_2\rangle$, a polyad ν is composed of all states such that $\nu_1+\nu_2 = \nu$

$N_{\max}, N_p \in \mathbb{N}^*$. This approximation then amounts to selecting combinations of the $N_{\max}$ lowest energy vibrational states with photonic excitations from 0 to $N_p - 1$ photons in the cavity. The eigenstates $|P_i\rangle$ of Hamiltonian (8), with energies $E_i(\lambda_c)$, are called polaritonic states, or more simply polaritons.

Within the cavity, the dipole moment $\boldsymbol{d}$ of the molecule is assumed aligned with the electric field $\boldsymbol{E}$ (molecular rotation is therefore frozen) such that the dipole moment can be approximated to first order with:

$$\begin{aligned} \hat{d} = \boldsymbol{d} \cdot \boldsymbol{E} &= d_0 + c_1 q_1 + c_2 q_2 \qquad & C_1 &= \frac{1}{\sqrt{2}}\left[\frac{c_1}{R'} + R' c_2\right] \\ &= d_0 + C_1 o_1 + C_2 o_2 \qquad & C_2 &= \frac{1}{\sqrt{2}}\left[-\frac{c_1}{R'} + R' c_2\right] \end{aligned} \tag{9}$$

where we set $R' = R\sqrt{\frac{1-a}{1+a}}$, d_0 corresponding to the permanent dipole and $C_i = \frac{\partial \hat{d}}{\partial o_i}$.

1.4. Numerical convergence study

The DVR method requires defining a spatial interval over which the Schrödinger equation will be solved. The particular form of the potential surface requires careful selection of this interval to avoid including an interval where the potential diverges toward $-\infty$. For this, a first convergence study is performed to determine the interval $(o_{\min}, o_{\max} = |o_{\min}| + 0.07)$ where the DVR method is applied to obtain the eigenstates of $h_i(o_i)$. The convergence criterion is based on the stability of the average energy $\langle E \rangle_n$ of the first n eigenstates of the isolated HH system, i.e., $|n_1, n_2\rangle$.

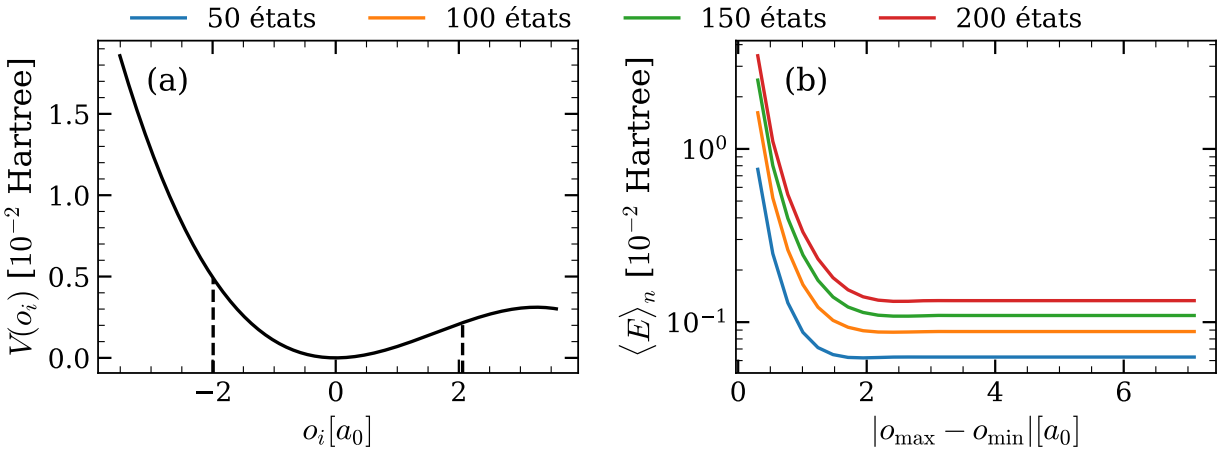

Figure 1: Convergence study according to the width of the interval $[o_{\min}, o_{\max}]$ for model 3.
(a) 1D potential with chosen interval (dotted line) for the DVR method.
(b) Average energy $\langle E \rangle_n$ of the first 50, 100, 150 and 200 states of the 2D system.

For model 2, the DVR method is applied over an interval $[-1.30, 1.38]$ and $[-2.02, 2.09]$ for model 3, values being in atomic units (a.u). For model 3, the selected interval does not include the entire potential up to the local maximum around 2.3 a.u (see figure 1.(a)). However, convergence of $\langle E \rangle_n$ is achieved over this interval where $|o_{\max} - o_{\min}| = 4.11$ a.u, and this for the first 200 states of the isolated HH system (see figure 1.(b)).

A final convergence study completes the basis $\mathcal{H}'$ by fixing the number of vibrational states $N_{\max}$ as well as the number of photons in the cavity N_p. To compare convergences, we introduce the average

value of energy gaps of the first n polaritons, denoted $\langle E(N_{\max}; N_p)\rangle$, as well as the relative gap between $\langle E(N_{\max}, N_p)\rangle$ and the value $\langle E(N_{\max} = 14; N_p = 17)\rangle$, denoted $\Delta\langle E(N_{\max}; N_p)\rangle$. These two study parameters are defined by:

$$\begin{aligned} \langle E(N_{\max}; N_p)\rangle &= \frac{1}{n}\sum_{i=1}^{n} E_i(\lambda_c = \lambda_{\max}) - E_0(\lambda_c = 0) \\ \Delta\langle E(N_{\max}; N_p)\rangle &= \frac{\langle E(N_{\max}; N_p)\rangle - \langle E(N_{\max} = 14; N_p = 17)\rangle}{\langle E(N_{\max} = 14; N_p = 17)\rangle} \end{aligned} \tag{10}$$

where $E_i(\lambda_c)$ is the energy of the i-th lowest energy polariton at coupling λ_c.

Only the first 10 polaritons will be studied for coupling λ_c from 0 to 0.15; the parameters introduced in (10) will therefore be taken at the maximum coupling value, i.e., $\lambda_c = 0.15$, and we choose to seek convergence for the first $n = 70$ polaritons.

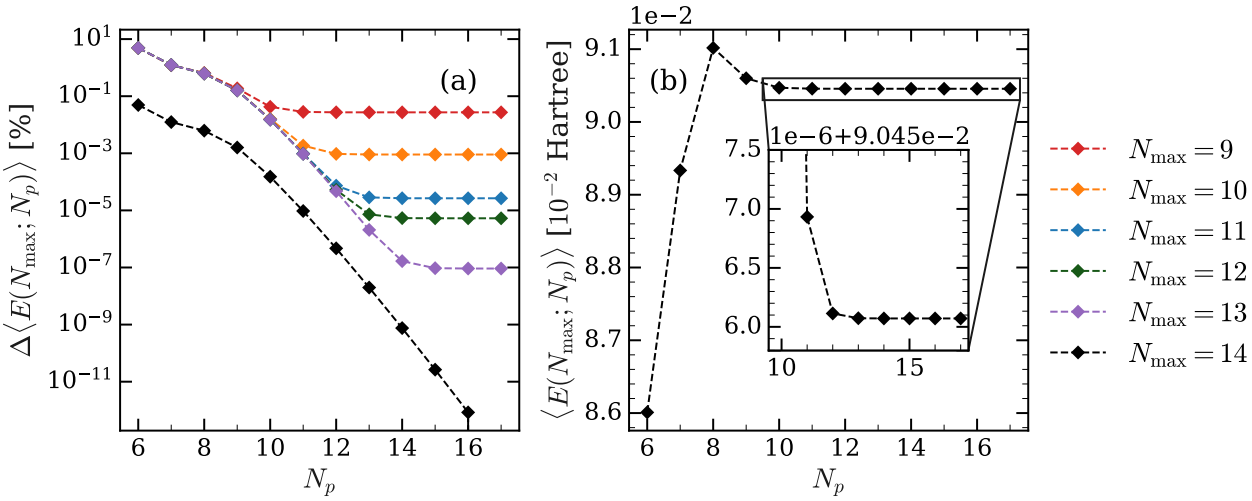

Figure 2: Convergence study on N_p of H_{PF} for the first 70 polaritons with model 3.
(a) Relative convergence of the average energy $\langle E(N_{\max}; N_p)\rangle$ compared to $N_{\max} = 14$.
(b) Absolute convergence of the average energy $\langle E(N_{\max}; N_p)\rangle$ for $N_{\max} = 14$.

Figure 2.(b) shows that for $N_{\max} = 14$, the energy gaps of the first 70 polaritons converge toward a fixed value of $E = 9.046.10^{-4}$ Hartree[2] To reduce computation time, it is favorable to reduce the basis size as much as possible by minimizing $N_{\max}$ and N_p, while maintaining a satisfactory degree of precision.

For this, figure 2.(a) compares relatively the convergence of energy gaps at other $N_{\max}$ compared to $N_{\max} = 14$. As expected, the relative gap is smaller the closer $N_{\max}$ approaches 14, ranging from 0.1% for $N_{\max} = 9$ to 10^{-7}% gaps for $N_{\max} = 13$. This gap in each case stabilizes around a fixed value, suggesting that even for other $N_{\max}$ values, the average energy gaps converge toward a fixed value close to the true value.

[2]The Hartree is the unit of energy in the atomic unit system and is defined as 1 Hartree = $2E_I$, where E_I is the ionization energy of the hydrogen atom.

In the continuation of this work, we chose to take $N_{\max} = N_p = 11$ to perform the static and dynamic simulations that will be presented in the next sections.

Similar convergence studies were performed to determine the parameters $N_{\max}, N_p$, and are reported in table 1 in the following section.

1.5. Model parameters, potential surface and wave functions

Parameters	Model 1	Model 2	Model 3
μ_1	1.0	1.0	1.0
μ_2	1.0	1.0	1.0
k_{112}	−0.078	−0.078	−0.039
k_{222}	−0.0078	−0.0078	−0.0078
k_{11}	0.3081	0.0829	0.0829
k_{22}	0.0893	0.3318	0.3318
$\omega_1(\text{cm}^{-1})$	2853.17	1480.45	1480.45
$\omega_2(\text{cm}^{-1})$	1536.32	2960.90	2960.90
N_{bs}	83	13	196
N_{max}	17	11	11
N_p	12	12	11
$\alpha_0(\text{degree})$	−8.73	9.74	9.74
μ	0.9539	0.9428	0.9428
μ_{12}	−3.1798	2.8284	2.8284
$U_{11} = U_{22}$	0.1759	0.1759	0.9652
U_{12}	0.1739	0.0586	0.3217
$U_{111} = U_{222}$	−0.0279	−0.0344	−0.0231
$U_{112} = U_{122}$	0.0104	0.0278	0.0147
d_0	0	0	0
c_1	0.1	0.1	0.1
c_2	0.05	0.05	0.05
C_1	0.114	0.103	0.124
C_2	−0.031	−0.043	−0.074

Table 1: Parameters in atomic units (a.u) of the Hamiltonian for the three models considered.

The complete set of parameters for the three models considered in this work is reported in table 1. For model 1, the cavity frequency $\omega_c = \omega_2$ is in resonance with the second vibrational excitation mode, and with the first vibrational excitation mode for models 2 and 3: $\omega_c = \omega_1$.

Here, only the case of a non-polar molecule is considered ($d_0 = 0$), with excitations on both modes ($c_1, c_2 \neq 0$). Between models 2 and 3, only the force constant k_{112} is divided by 2, reducing the coupling between the first mode along o_1 and the second mode along o_2.

In all three cases, the potential $V(o_1, o_2)$ is symmetric about the axis $o_2 = o_1$ (see figure 3), the minimum at O and the maximum at A on the symmetry axis, and the saddle points S_1, S_2 symmetric.

The first excited wave functions are presented in Appendix B. For model 1, counting nodes along each axis allows determining the number of excitation quanta along each mode in the manner of atomic orbitals $1s, 2s, 3s, ...$

For models 2 and 3, the nodal structure is difficult to interpret because each wave function is a linear combination of different pure vibrational excitations due to Fermi coupling. Only the wave function without excitation and the first excited wave function are identifiable because they preserve quasi-pure decompositions on a single vibrational state.

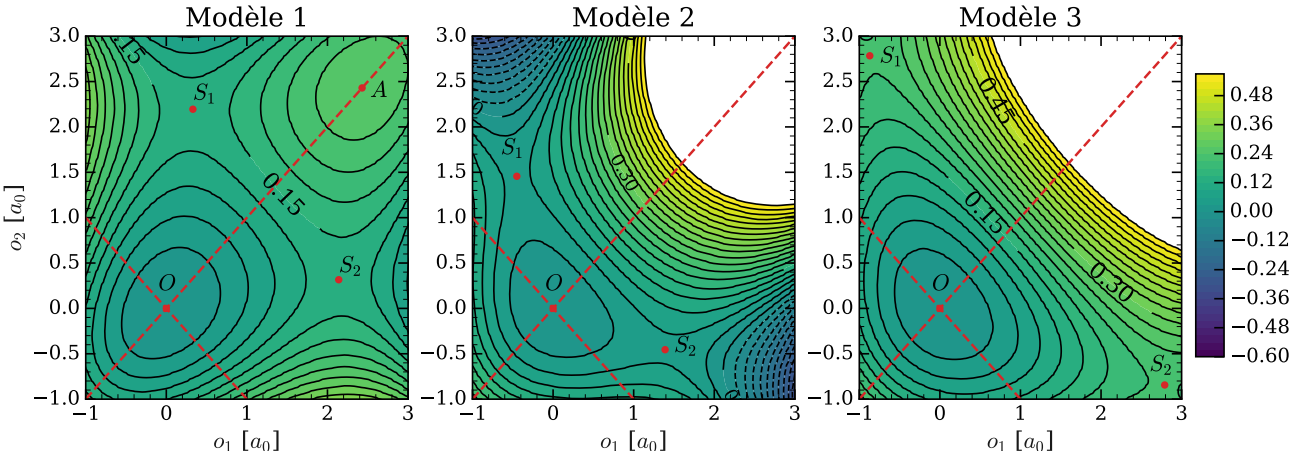

Figure 3: Potential energy surface of models 1 to 3.

1.6. System properties in static and dynamic

The polaritonic states $|P_i\rangle$ decompose in $\mathcal{H}'$ such that:

$$|P_i\rangle = \sum_{n_p=0}^{N_p-1} \sum_{n_1}^{N_{\max}-1} \sum_{n_2}^{N_{\max}-1} c^{(i)}_{n_p,n_1,n_2} |n_p, n_1, n_2\rangle \tag{11}$$

The average number of photons $\langle n_p \rangle_i$, the moments $\langle o_1^n o_2^m \rangle_i$ and the presence probability $\langle P_n \rangle_i$ in a polyad[3] $n = n_1 + n_2$ are thus defined:

$$\langle P_n \rangle_i = \sum_{n_p} \sum_{n_1}^{n} \left| c^{(i)}_{n_p,n_1,n-n_1} \right|^2 \tag{12}$$

$$\langle n_p \rangle_i = \langle P_i | a^\dagger a | P_i \rangle = \sum_{n_p,n_1,n_2} n_p \left| c^{(i)}_{n_p,n_1,n_2} \right|^2 \tag{13}$$

$$\langle o_1^n o_2^m \rangle_i = \langle P_i | o_1^n o_2^m | P_i \rangle = \sum_{\boldsymbol{n},\boldsymbol{n}',n_p} c^{(i)}_{n_p,n_1,n_2} c^{(i)}_{n_p,n_1',n_2'} \langle n_1 | o_1^n | n_1' \rangle \langle n_2 | o_2^m | n_2' \rangle \tag{14}$$

As mentioned in the previous section 1.5., the eigenwave functions are distributed largely along the axes $o_1 = \pm o_2$, which motivates introducing the parameters $\langle o_\pm \rangle_i$ and $\langle \Delta_\pm \rangle_i$:

$$\langle o_\pm \rangle_i = \langle o_1 \rangle_i \pm \langle o_2 \rangle_i \qquad \langle \Delta_\pm \rangle_i = \sqrt{\langle o_\pm^2 \rangle_i - \langle o_\pm \rangle_i^2} \tag{15}$$

Consider a non-stationary quantum state $|\Psi(t=0)\rangle = |0, n_1, n_2\rangle$ prepared at $t = 0$ and $\lambda_c = 0$ with:

$$|\Psi(t=0)\rangle = \sum_i b_i(0) |P_i\rangle \tag{16}$$

Since the Hamiltonian (8) does not explicitly depend on time, integrating the time-dependent Schrödinger equation leads directly to the expression for $|\Psi(t)\rangle$:

$$|\Psi(t)\rangle = \sum_i b_i(0) e^{-E_i t} |P_i\rangle = \sum_{n_p,\boldsymbol{n}} \underbrace{\sum_i b_i(0) e^{-iE_i t} c^{(i)}_{n_p,\boldsymbol{n}}}_{c_{n_p,\boldsymbol{n}}(t)} |n_p, \boldsymbol{n}\rangle \tag{17}$$

From the expression of $|\Psi(t)\rangle$, the previously defined static parameters are obtained dynamically:

$$\begin{aligned}
\langle n_p \rangle(t) &= \sum_i b_i^2(0) \langle n_p \rangle_i + 2 \sum_i \sum_{j>i} b_i(0) b_j^*(0) \cos\big((E_j - E_i)t\big) \langle P_i | a^\dagger a | P_j \rangle \\
\langle o_1^n o_2^m \rangle(t) &= \sum_i b_i^2(0) \langle o_1^n o_2^m \rangle_i + 2 \sum_i \sum_{j>i} b_i(0) b_j^*(0) \cos\big((E_j - E_i)t\big) \langle P_i | o_1^n o_2^m | P_j \rangle \\
\langle P_n \rangle(t) &= \sum_{n_p}^{N_p-1} \sum_{n_1}^{n} \left| c_{n_p,n_1,n-n_1}(t) \right|^2 \\
&= \sum_{n_p}^{N_p-1} \sum_{n_1}^{n} \sum_i b_i^2(0) \left| c^{(i)}_{n_p,n_1,n-n_1} \right|^2 \\
&\quad + 2 \sum_{n_p}^{N_p-1} \sum_{n_1}^{n} \sum_i \sum_{j>i} b_i(0) c^{(i)}_{n_p,n_1,n-n_1} b_j^*(0) c^{(j)}_{n_p,n_1,n-n_1} \cos\big((E_j - E_i)t\big)
\end{aligned} \tag{18}$$

[3] States $|0,2,3\rangle$ and $|2,1,4\rangle$ are two examples of states belonging to polyad $n = 5$

2. Fermi Resonance ($\Delta = 0$)

2.1. Isolated Hénon-Heiles System ($N_p = 0$)

In table 2, the eigenmodes of polyads $\nu = \nu_1 + \nu_2$ for $\nu = 0 - 4$ are reported along with the presence probabilities in each polyad for each eigenmode. The assignments of couples (ν_1, ν_2) are guided by the probabilities $\langle P_\nu \rangle_i$ for the first four eigenmodes, and by $\langle \Delta_\pm \rangle$ for the remaining modes.

In the case of model 1, assignment could be performed by counting nodes on the eigenwave functions along each axis o_i. For models 2 and 3, the eigenwave functions being mixtures of pure vibrational excitations, assignment by wave functions is no longer effective, and therefore becomes arbitrary for the last modes.

(ν_1, ν_2)	Energy (10^{-2} Hartree)	$\langle P_0 \rangle_i$	$\langle P_1 \rangle_i$	$\langle P_2 \rangle_i$	$\langle P_3 \rangle_i$	$\langle P_4 \rangle_i$	$\langle \Delta_- \rangle_i$ (a_0)	$\langle \Delta_+ \rangle_i$ (a_0)
(0, 0)	0.000	1.000	0.000	0.000	0.000	0.000	0.240	0.240
(1, 0)	0.670	0.000	1.000	0.000	0.000	0.000	0.417	0.240
(2, 0)‘	1.310	0.000	0.441	0.559	0.000	0.000	0.448	0.327
(0, 1)‘	1.375	0.000	0.557	0.442	0.000	0.000	0.387	0.352
(3, 0)‘	1.952	0.000	0.000	0.472	0.527	0.000	0.566	0.331
(1, 1)‘	2.065	0.000	0.000	0.525	0.474	0.000	0.516	0.349
(4, 0)‘	2.582	0.000	0.000	0.086	0.497	0.416	0.637	0.362
(0, 2)‘	2.687	0.000	0.001	0.728	0.015	0.255	0.426	0.478
(2, 1)‘	2.768	0.000	0.000	0.179	0.490	0.330	0.544	0.402

Table 2: Eigenvalues of the first nine bound states of the free HH system (model 3) for $N_1 = N_2 = 11$ with state assignment, probability $\langle P_\nu \rangle_i$ and $\langle \Delta_\pm \rangle_i$.

The ground level (0, 0) and the first excited level (1, 0) are assigned by counting nodes on their wave functions (see figure 8) having respectively no nodes and a single node. The assignments are confirmed by the values $\langle P_0 \rangle \approx 1$ for (0, 0) and $\langle P_1 \rangle \approx 1$ for (1, 0) (see table 2). These two states are therefore completely decoupled from other states.

All other states decompose over different polyads with at minimum two non-zero $\langle P_n \rangle$ values, which is the effect of Fermi resonance in the system. The next two states (2, 0)‘ and (0, 1)’ decompose over polyads $n = 1$ and 2 ($\langle P_1 \rangle \neq 0$ and $\langle P_2 \rangle \neq 0$). These two states decompose mainly over (2, 0) and (0, 1), which led to introducing the notation $(n, m)'$ to specify that the state is a mixture of different excitations. Analogous observations repeat for the following states, except for the distribution over polyads which changes.

Note that the higher the energy, the more likely the probability of decomposing over a polyad with large n. Naturally, as energy increases, a state can be more excited and therefore be in a higher polyad.

Identical observations were noted in the case of model 2. For model 1, all states are almost pure, as shown in figure 8 (Appendix B) where the nodal structure is clearly identifiable, unlike models 2 and 3.

2.2. Hénon-Heiles System in Cavity ($N_p \neq 0$)

In table 3, for $\lambda_c = 0$, the first thirteen polaritonic states are assigned using their $\langle \Delta_{\pm} \rangle$ values compared to the vibrational assignments in table 2.

Polaritonic State	$\lvert n_p, n_1, n_2 \rangle$	$(E_i - E_0)/\omega_c$
$\lvert P_0 \rangle$	$\lvert 0,0,0 \rangle$	0.000
$\lvert P_1 \rangle$	$\lvert 0,1,0 \rangle$	1.000
$\lvert P_2 \rangle$	$\lvert 1,0,0 \rangle$	1.000
$\lvert P_3 \rangle$	$\lvert 0,(2,0)' \rangle$	1.954
$\lvert P_4 \rangle$	$\lvert 2,0,0 \rangle$	2.000
$\lvert P_5 \rangle$	$\lvert 1,1,0 \rangle$	2.000
$\lvert P_6 \rangle$	$\lvert 0,(0,1)' \rangle$	2.052
$\lvert P_7 \rangle$	$\lvert 0,(3,0)' \rangle$	2.912
$\lvert P_8 \rangle$	$\lvert 1,(2,0)' \rangle$	2.954
$\lvert P_9 \rangle$	$\lvert 3,0,0 \rangle$	3.000
$\lvert P_{10} \rangle$	$\lvert 2,1,0 \rangle$	3.000
$\lvert P_{11} \rangle$	$\lvert 1,(0,1)' \rangle$	3.052
$\lvert P_{12} \rangle$	$\lvert 0,(1,1)' \rangle$	3.081

Table 3: Assignment of the first thirteen polaritonic states and relative eigenvalues without field ($\lambda_c = 0$).

These first thirteen polaritons are built on vibrational excitations from polyads $n = 0$ to 3, and photonic states with at most 3 photons. The energies of these polaritons are distributed from 0 to $3\omega_c$.

The ground level $|P_0\rangle$ is as expected a state without any photonic or vibrational excitation. The next two polaritonic states, $|P_1\rangle$ and $|P_2\rangle$, are degenerate at energy ω_c. $|P_1\rangle$ is a purely vibrational state $(1,0)$ and $|P_2\rangle$ a purely photonic state. The degeneracy of these two states is due to choosing the first excited level (1, 0) of energy ω_1 in resonance with the cavity (see section 1.5.).

For each potential model, we focused on polaritonic states around $2\omega_c$, i.e., polaritonic states $|P_3\rangle$ to $|P_6\rangle$. This energy interval is of interest for observing interactions between different vibrational excitation modes. The mode where the first excited level $|0,1,0\rangle$ is in resonance with ω_c will appear around $2\omega_c$ in a simple form with a single photon of the same energy $|1,1,0\rangle$ but also in a second doubly excited form $|0,(2,0)'\rangle$. A photonic state also appears with two photons $|2,0,0\rangle$ at $2\omega_c$. Finally, the first excited level $|0,0,1\rangle$ of the second mode appears, the latter having been chosen to be strictly at energy $2\omega_c$.

In such a configuration, and without interaction with the cavity ($\lambda_c = 0$), the four states $|0,2,0\rangle$, $|2,0,0\rangle$, $|1,1,0\rangle$ and $|0,0,1\rangle$ should be four states at the same energy $2\omega_c$: each photon and each excitation along the first mode having energy ω_c, and $2\omega_c$ for each excitation in the second mode.

Instead of obtaining four degenerate states at $\lambda_c = 0$, table 3 gives two degenerate states $|P_4\rangle = |2,0,0\rangle$ and $|P_5\rangle = |1,1,0\rangle$ at the same energy $2\omega_c$, and two states $|P_3\rangle = |0,(2,0)'\rangle$ and $|P_6\rangle = |0,(0,1)'\rangle$ at respective energies of 1.954 ω_c and 2.052 ω_c, i.e., a gap of about 0.05 ω_c from the expected value $2\omega_c$. These last two states are mixtures of vibrational excitations: (2, 0), (0, 2), (0, 1) and (1, 1). This mixture then allows the affected states to move positively or negatively away from $2\omega_c$ according to the intensity of the resonance.

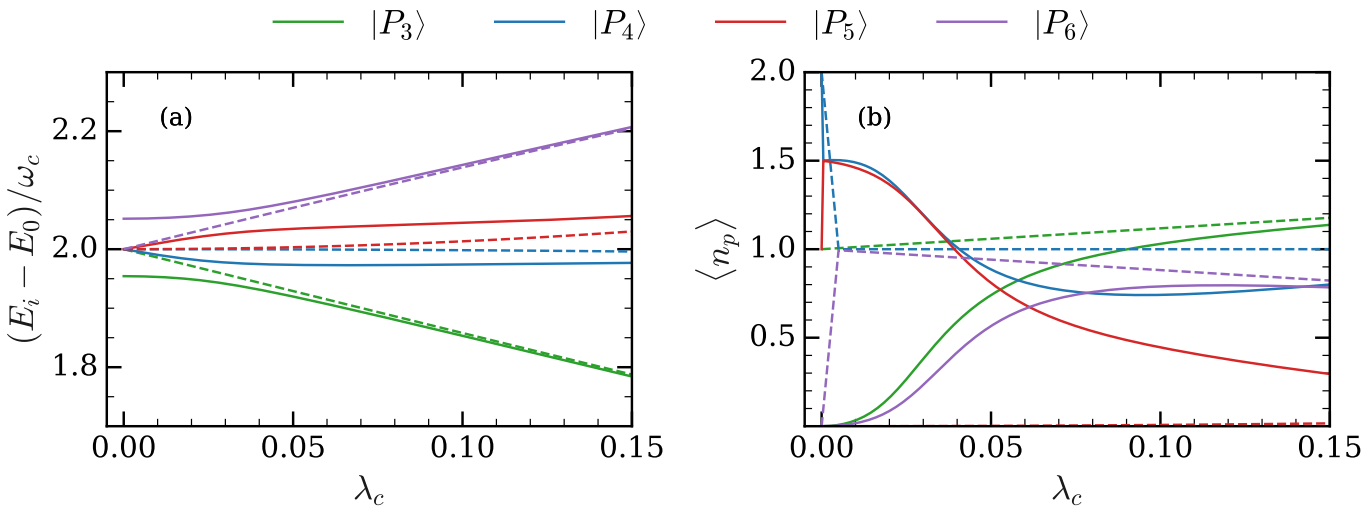

Figure 4: Evolution of polaritons $|P_i\rangle$ for model 3 and in the harmonic limit (dotted line). (a) Eigenvalues of polaritons $|P_i\rangle$; (b) Average number of photons $\langle n_p \rangle$ according to λ_c.

This splitting structure is comparable to a Fermi resonance, where the strong energy proximity of the two uncoupled states as well as the potential symmetry authorize the manifestation of such a resonance. The system thus reduces its level of degeneracy around $2\omega_c$ by this energy splitting of states.

When λ_c increases, polaritons $|P_3\rangle$ to $|P_6\rangle$ progressively interact, consequently increasing the energy gap of the Fermi resonance (see figure 4.(a)). For large λ_c, the system energies in the anharmonic case tend toward the energies of the harmonic case (represented by dotted lines). Given the Hamiltonian (8) of the system in cavity, at low λ_c, the system is dominated by vibrational and photonic excitations as well as potentials V_2 and V_3. Conversely, at high λ_c, dipolar interactions dominate the system, and energies then tend to approach the harmonic case, which is consistent with the observation previously made in figure 4.(a).

In figure 4.(b), the decreases in average number of photons $\langle n_p \rangle$ for $|P_4\rangle$ and $|P_5\rangle$ are associated with increases in number of photons for $|P_3\rangle$ and $|P_6\rangle$ with quasi-exact conservation of three photons regardless of λ_c (a slight continuously increasing variation of 0.3% of the total average number is noted between $\lambda_c = 0$ and $\lambda_c = 0.15$). The harmonic case is also represented by dotted lines and underlines the major role that anharmonicity of the potential surface plays on the system eigenstates. In particular, it cancels the Fermi structure.

This energy and photonic evolution where states interact with each other indicates that the evolution of these states occurs mainly within the space formed by these states.

In model 2, which is a similar model where anharmonicity is more pronounced (k_{112} being twice as large as for model 3), the Fermi structure in the case of model 3 presents a smaller energy splitting than for model 2. The parameter k_{112} thus defines the intensity of the Fermi resonance: the larger k_{112}, the larger the energy splitting. Finally, model 3 was studied in the case where ω_c is not in exact resonance with the first excited level ($\Delta \neq 0$). As for model 1, no crossing of polariton energies could be recorded for all studied values of Δ (see figure 9 in Appendix C).

2.3. Dynamic Behavior

After studying the static evolution of system eigenstates as a function of coupling with the cavity, the states forming the Fermi doublet are studied dynamically. Two quantum simulations are performed by preparing two systems in respective states $|\Psi(t=0)\rangle = |0,(2,0)'\rangle$ and $|\Psi(t=0)\rangle = |0,(0,1)'\rangle$, for $\lambda_c = 0.01, 0.05$ and 0.09. These states at $t=0$ are defined at $\lambda_c = 0$, so they are not eigenstates of the system for the considered λ_c values. In each case, quantum decoherence problems are neglected, and we assume no perturbations or interactions are present. These simulations are represented in figures 5 and 6.

In figures 5 and 6, for low coupling $\lambda_c = 0.01$, the quantum trajectory of both systems remains confined around their initial vibrational states. In both cases, the average number of cavity photons $\langle n_p \rangle$ remains around zero, confirming the absence of state transitions for these two systems. The weak coupling of vibrational excitations with the electromagnetic field does not allow redistribution of vibrational excitations on the molecule, nor emission-absorption of photons.

In figure 5, for intermediate coupling $\lambda_c = 0.05$, a state transition oscillation period of about 475 fs is noted. Over a 4ps quantum trajectory, the system is able to transition almost completely toward state $(0,1)'$ as shown in figure 5.(a). Transitions toward mixtures where (0, 0) and (1, 0) are equiprobable are noted with the trajectory reaching the middle of the segment between these two states. An equivalent transition toward a mixture (1, 0) and (3, 0)‘ is present with stronger weight on state (1, 0), the trajectory being on the segment connecting the two states, but closer to (1, 0). For the strongest considered coupling $\lambda_c = 0.09$, a similar transition oscillation period of 475 fs is noted. The system performs transitions toward the same vibrational states as for $\lambda_c = 0.05$ with the difference that the system now performs complete transitions for (0, 1)’, (0, 0) and (1, 0).

In figure 6, for $\lambda_c = 0.05$, an oscillation period of 1000 fs is noted versus 250 fs for $\lambda_c = 0.09$. For intermediate coupling, only one quasi-complete transition is observed, where the system oscillates between a pure (0, 1)‘ state (the initial state) and toward an equiprobable mixture of (0, 0) and (1, 0). To perform this transition, the system must emit one photon to pass from (0, 1)’ to (1, 0) and two photons to pass to (0, 0), i.e., an average number of photons of one and a half knowing that the transition toward (1, 0) or (0, 0) is equiprobable. In the case of the reverse transition, the system must then absorb photons from the cavity to return to (0, 1)‘. Figure 6.(b) for $\lambda_c = 0.05$ is consistent with the previous statement, with oscillation of the average number of photons between zero and one and a half. For $\lambda_c = 0.09$, the system can no longer transition completely toward other states.

For each quantum trajectory, transitions respect energy conservation either by emission or by absorption of photons during vibrational energy exchanges.

In both cases, and for sufficiently large coupling λ_c, vibrational energy redistributions between modes are observed. These redistributions would then allow selective control of reactive pathways where preparing a molecule in a well-defined state, and subjected to well-chosen coupling and potential would allow controlling vibrational transitions like the $\lambda_c = 0.05$ case in figure 6, where the state oscillates between two defined states. However, these dynamic results obtained on time scales on the

order of picoseconds are only valid if this time is short compared to the decoherence time linked to collisions as well as photon loss in the Fabry-Perot cavity.

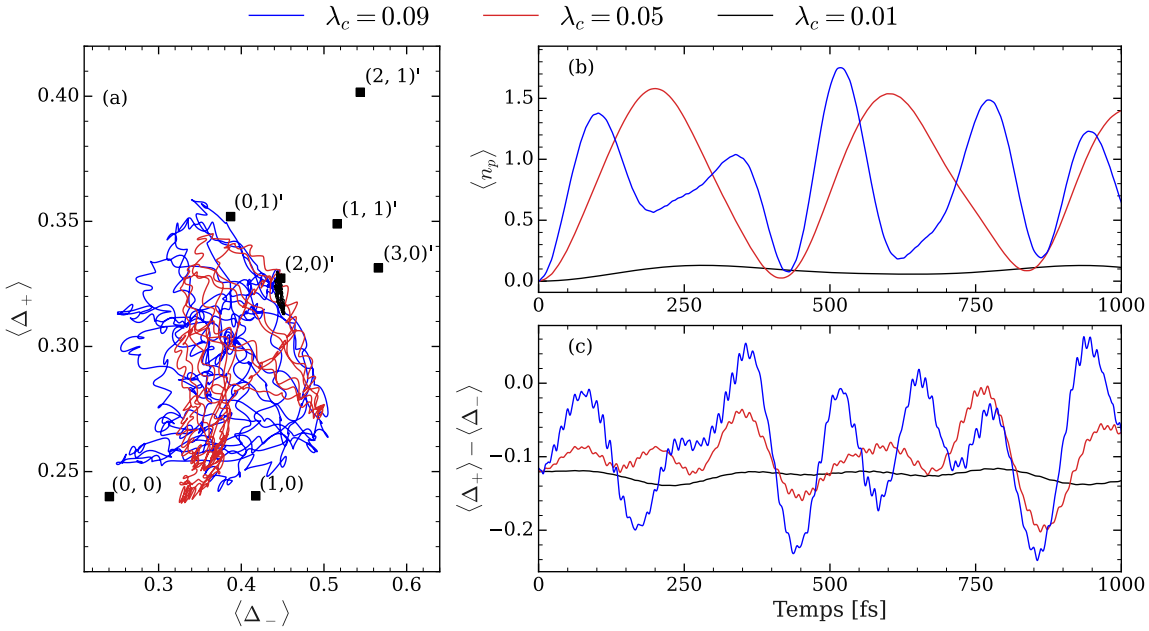

Figure 5: Temporal evolution of the system starting from $|P_3\rangle = |0, (2,0)'\rangle$.

(a) System trajectory over 2ps every 0.5fs with position of known states.

(b) Average number of photons in the system over 1ps.

(c) Dispersion difference $\langle \Delta_+ \rangle - \langle \Delta_- \rangle$ of the system over 1ps.

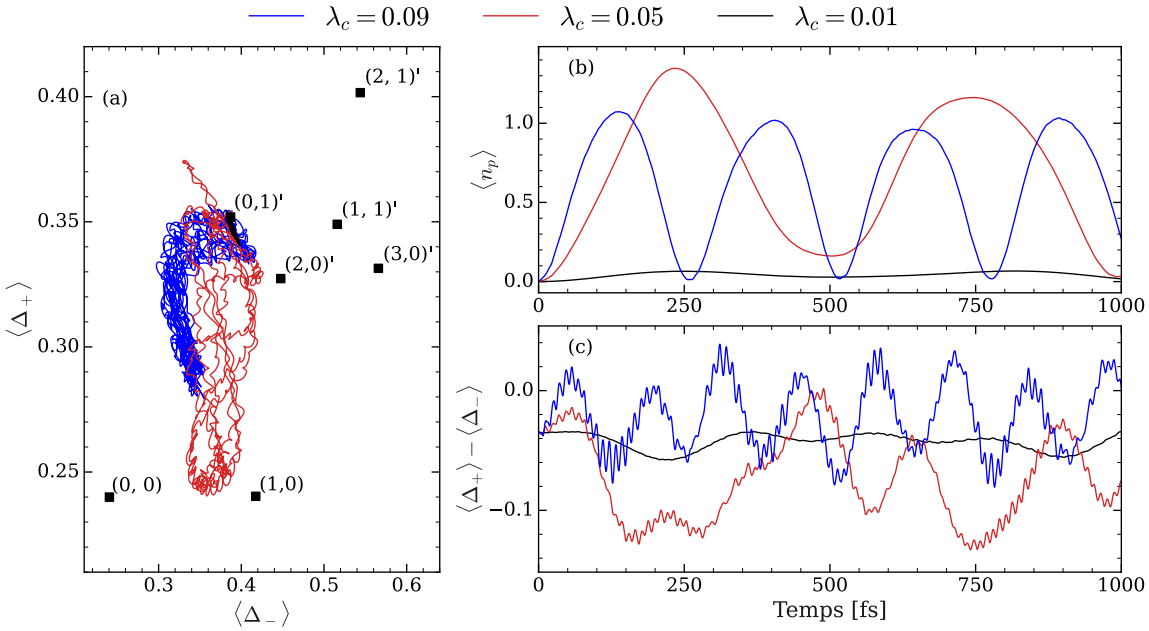

Figure 6: Temporal evolution of the system starting from $|P_6\rangle = |0, (0,1)'\rangle$.

(a) System trajectory over 2ps every 0.5fs with position of known states.

(b) Average number of photons in the system over 1ps.

(c) Dispersion difference $\langle \Delta_+ \rangle - \langle \Delta_- \rangle$ of the system over 1ps.

3. Extension of the System to N Molecules

3.1. Hamiltonian for N Molecules

After studying the two possible resonance modes for a molecule with two degrees of freedom in the first half of this internship, theoretical work is proposed to extend the model to N molecules. Each molecule retains its Hamiltonian H_{PF}, but photonic exchange terms and coupling between molecular dipoles must be added.

The Hamiltonian of a polaritonic system composed of N molecules is given by:

$$H = \sum_{i=1}^{N} H_{\text{HH}}^{(i)} + \omega_c a^\dagger a + \frac{\lambda_c \omega_c}{d_{01}} D\big(a^\dagger + a\big) + \frac{\lambda_c^2 \omega_c}{d_{01}^2} D^2 \tag{19}$$

where we define $a = \frac{1}{\sqrt{N}} \sum_i a_i$ as well as its adjoint $a^\dagger$ with the prefactor $\frac{1}{\sqrt{N}}$ to preserve the commutation relation of the ladder operator, and $D = \sum_i d_i$ the total dipolar operator of the system. The a_i are the ladder operators and d_i the dipolar operators for the i-th molecule.

By expanding the terms, the Hamiltonian H is written:

$$H = \sum_{i=1}^{N} H_{\text{PF}}^{(i)} + \sum_{i=1}^{N} \sum_{j \neq i}^{N} V^{(i,j)}, \qquad V^{(i,j)} = \frac{\omega_c}{N} a_i^\dagger a_j + \frac{\lambda_c \omega_c}{d_{01}\sqrt{N}} d_i \big(a_j^\dagger + a_j\big) + \frac{\lambda_c^2 \omega_c}{d_{01}^2} d_i d_j \tag{20}$$

with:

$$H_{\text{PF}}^{(i)} = H_{\text{HH}}^{(i)} + \frac{\omega_c}{N} a_i^\dagger a_i + \frac{\lambda_c \omega_c}{d_{01}\sqrt{N}} d_i \big(a_i^\dagger + a_i\big) + \frac{\lambda_c^2 \omega_c}{d_{01}^2} d_i^2 \tag{21}$$

where $H_{\text{PF}}^{(i)}$ is the Pauli-Fierz Hamiltonian of the i-th molecule considered individually. The cross terms, arising from expansions of $a^\dagger a$, $D\big(a^\dagger + a\big)$ and D^2, are integrated into $V^{(i,j)}$ and represent photonic and vibrational exchange terms between molecules.

The eigenvectors $\left|P_k^{(i)}\right\rangle$ and eigenvalues $\varepsilon_k^{(i)}$ of $H_{\text{PF}}^{(i)}$ are calculated. For a system of N identical particles, we consider the basis $|p_1 p_2 ... p_N\rangle \equiv \left|P_{p_1}^{(1)}\right\rangle \otimes \left|P_{p_2}^{(2)}\right\rangle \otimes ... \left|P_{p_N}^{(N)}\right\rangle$ where $p_i \in [\![0; N_{\text{pol}}]\!]$.

The basis size of Hamiltonian H is classically $\left(N_{\text{max}}^2 N_p\right)^N$. The explosion of basis size with the number of molecules N leads to introducing the previous parameter N_{pol}. This allows considering only the first N_{pol} polaritons of individual Hamiltonians for the N-molecule basis, reducing the size to $\left(N_{\text{pol}}\right)^N$, where $N_{\text{pol}} \in [\![1; N_{\text{max}}^2 N_p]\!]$.

To continue reducing the problem size, two constraints are added on energy as well as the total number of excitations on the N-molecule state. Only states $|p_1, p_2, ..., p_N\rangle$ having energy $\varepsilon = \sum_k \varepsilon_{p_k}$ less than ε_c and whose cumulative number of photonic and vibrational excitations is less than a parameter n_c are retained in the final basis.

The matrix elements of the final N-molecule Hamiltonian are then deduced:

$$\begin{aligned} \langle p_1 p_2 ... | H | p_1' p_2' ... \rangle &= \sum_{i=1}^{N} \left\langle p_1 p_2 ... \middle| H_{\text{PF}}^{(i)} \middle| p_1' p_2' ... \right\rangle + \sum_{i=1}^{N} \sum_{j \neq i}^{N} \left\langle p_1 p_2 ... \middle| V^{(i,j)} \middle| p_1' p_2' ... \right\rangle \\ &= \sum_{i=1}^{N} \left(\varepsilon_{p_i} \prod_{j \neq i} \delta(p_j, p_j') \right) + \sum_{i=1}^{N} \sum_{j \neq i}^{N} \left\langle p_1 p_2 ... \middle| V^{(i,j)} \middle| p_1' p_2' ... \right\rangle \end{aligned} \tag{22}$$

The matrix elements of coupling $V^{(i,j)}$ are written:

$$\begin{aligned}\left\langle p_1 p_2 ... \middle| V^{(i,j)} \middle| p_1' p_2' ... \right\rangle = & \frac{\omega_c}{N} \left\langle p_i p_j \middle| a_i^\dagger a_j \middle| p_i' p_j' \right\rangle I(i,j) \\ & + \frac{\lambda_c \omega_c}{d_{01}\sqrt{N}} \left\langle p_i p_j \middle| d_i \left(a_j + a_j^\dagger \right) \middle| p_i' p_j' \right\rangle I(i,j) \\ & + \frac{\lambda_c^2 \omega_c}{d_{01}^2} \left\langle p_i p_j \middle| d_i d_j \middle| p_i' p_j' \right\rangle I(i,j)\end{aligned} \tag{23}$$

where

$$I(i,j) = \prod_{k \neq i,j} \delta(p_k, p_k') \tag{24}$$

ensures collinearity of other vectors of non-coupled molecules.

The different matrix elements for $V^{(i,j)}$ can be obtained[4] from:

$$\begin{aligned}\left\langle p_i \middle| a_i^\dagger \middle| p_i' \right\rangle &= \sum_{n_p', n_1', n_2'} c^k_{n_p'+1, n_1', n_2'} c^{k'}_{n_p', n_1', n_2'} \sqrt{n_p' + 1} \\ \langle p_i | a_i | p_i' \rangle &= \sum_{n_p', n_1', n_2'} c^k_{n_p'-1, n_1', n_2'} c^{k'}_{n_p', n_1', n_2'} \sqrt{n_p'}\end{aligned} \tag{25}$$

The dipole moment matrix elements are calculated numerically, since the states are not decomposed in the basis of harmonic oscillator eigenvectors, no analytical calculation is therefore possible.

The second part of the work was to implement the calculations of all the previously introduced matrix elements, and to adapt the existing Fortran codebase of Mr. Pascal Parneix for single-molecule simulations to obtain N-molecule simulations.

The major work was to individually verify that the routines calculating matrix elements return expected results.

First simulations for different numbers of molecules N could be conducted in which behavior similar to what is expected was observed. By fixing the parameter $\varepsilon_c = 1.1$ to focus on the first polariton block, each simulation returns $N-1$ non-physical (antisymmetric under photon exchange) states, 2 symmetric states, as well as $N-1$ states called "dark states" that are not coupled to the cavity. These results are consistent knowing that there are many more combinations to create an antisymmetric state than a symmetric one. Experimentally, dark states are also much more numerous than physical states, which significantly complicates observation of physical states.

Unfortunately, convergence problems remain, where by limiting $\varepsilon_c = 1.1$ to study the first polariton block, and moving to $\varepsilon_c = 2.2$ to move to the second polariton block, we observed that the eigenvalues of the N-molecule system varied significantly. Work on this subject remains to be continued to ensure the validity of the routines I programmed.

[4]By noting the orthonormalization of Fock states where $\langle n_p | n_p' \rangle = \delta_{n_p, n_p'}$, and similarly for vibrational excitations: $\langle n_i | n_i' \rangle = \delta_{n_i, n_i'}$. These properties are satisfied in our simulations, where $\langle n_i | n_i' \rangle \approx 10^{-27}$.

4. Conclusion and Work Perspectives

The light-matter coupling between a mode ω_c of the electromagnetic field of a Fabry-Perot cavity and a linear triatomic molecule modeled by a Hénon-Heiles potential led to the formation and study of polaritonic states, i.e., hybrid states linking light and matter. Different forms of resonance could be investigated under different models (1, 2 and 3), including models 1 and 2 which should be the subject of a future article by Mr. Pascal Parneix, and model 3 which was the subject of this report.

The cavity resonance with the first vibrational mode highlighted the appearance of a Fermi structure, commonly observed in infrared spectroscopy probing molecular vibrational modes.

The polaritonic states constituting the Fermi structure could be studied by preparing systems in these states, and by following the evolution of these systems over time. Demonstrating different vibrational energy redistributions between modes for the same initial state showed the influence of coupling λ_c on the temporal evolution of the system. These redistributions could then allow controlling the reactivity of molecules within Fabry-Perot micro-cavities.

Finally, the model was extended for an N-molecule system, and the single-molecule simulation codebase was adapted for N molecules. Preliminary results that remain to be validated were obtained and seem to be in a promising direction. However, convergence problems were raised during the last week, and these have not been resolved so far. The continuation of work would then be to pursue verifications of the N-molecule program and the validity of proposed hypotheses to restrict the problem dimension.

On a more personal note, this internship was my first interaction with the research world, and although it would be exaggerated to be able to fully measure what research work is, this experience can only comfort me in my desire to continue and hope to one day be able to contribute in turn to understanding and extending knowledge of Physics. During these few weeks, the oscillations between the satisfaction of advancing, understanding a little more than the day before the study subject, then the lows where I struggled to understand certain notions, the multiple hours searching for the origin of a Fortran code error, or having to debug a segmentation error could seem hard, but the satisfaction of finally succeeding in understanding or unblocking the program are well worth the few difficulties to achieve it. This internship was an opportunity to leave my usual languages and encounter one of the most atypical[5] languages I have had the opportunity to encounter so far: Fortran. This will be added to other languages that accompany me in studies so far like C, Python and Julia.

On the human level, thank you again to the people I met during this internship, and more particularly to Pascal Parneix for supervising me during this internship, but also for his warm welcome and the confidence he accorded me. Thank you for everything.

[5]Atypical for its different syntax from other languages and sometimes 'surprising'

Appendix A

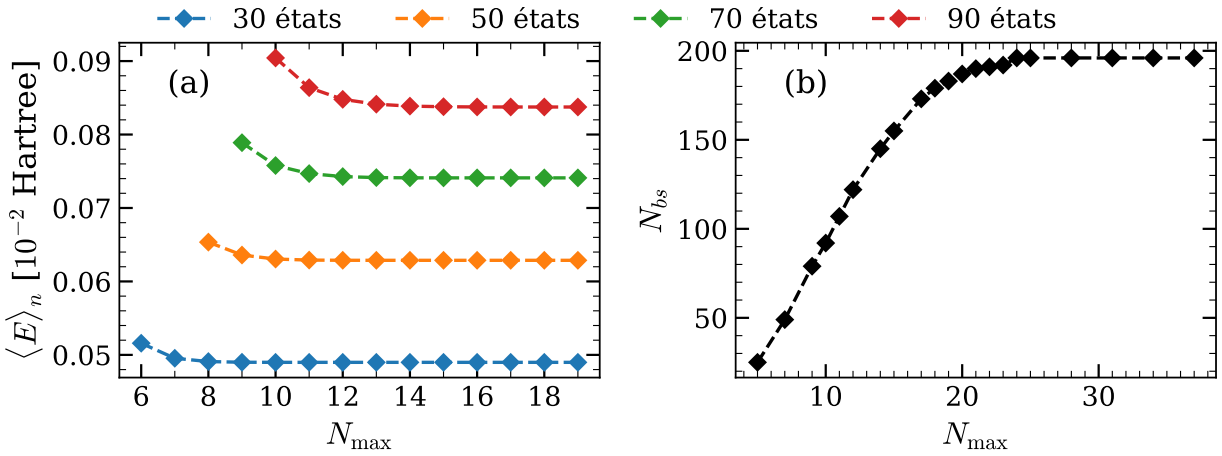

Figure 7: Convergence study on $N_{\max}$ of the isolated HH system for model 3 ($k_{112} = -0.05$). (a) Convergence of average energy $\langle E \rangle$ of the first 30, 50, 70 and 90 states of the 2D system. (b) Convergence of the number of bound states N_{bs}.

Appendix B

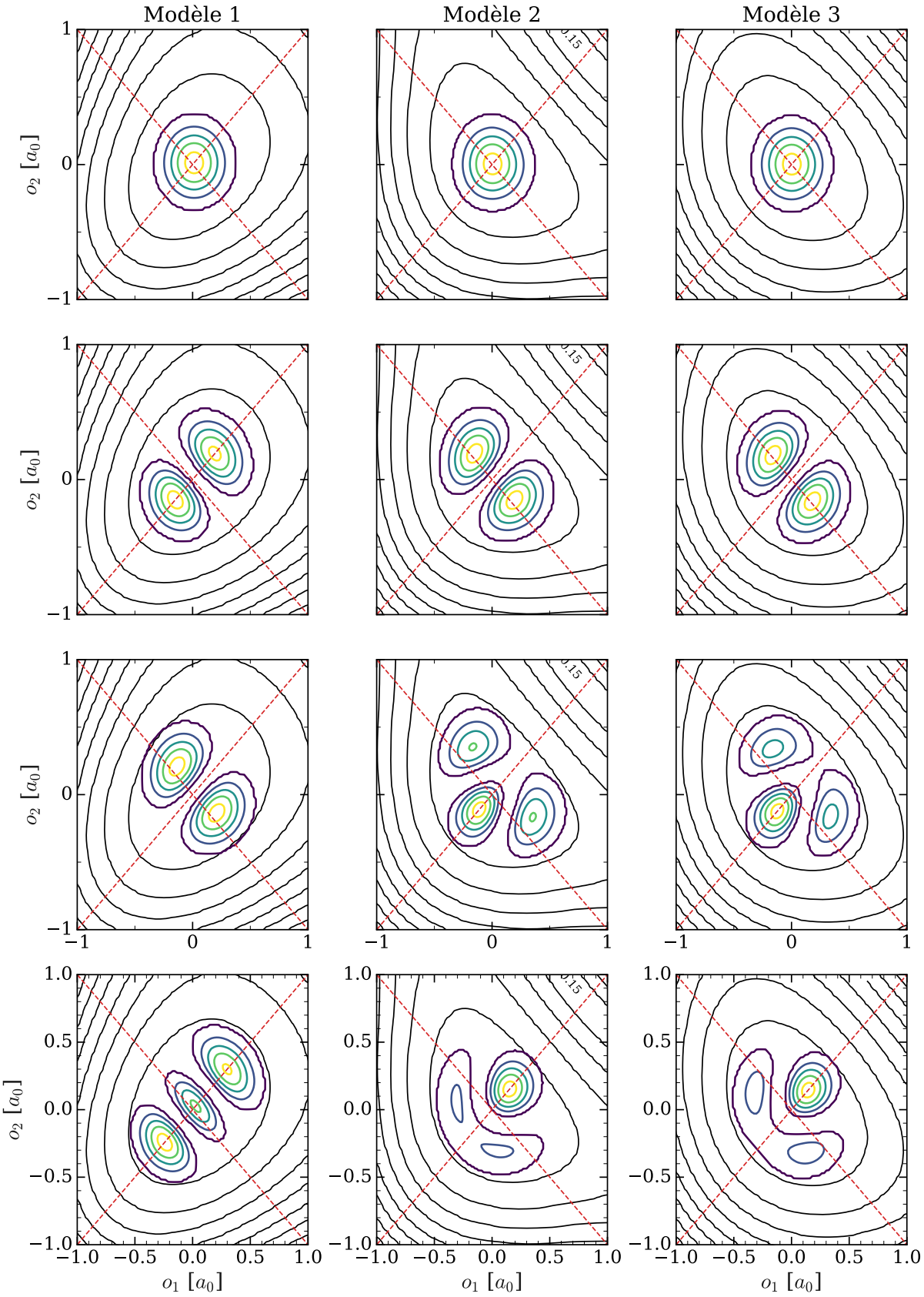

Figure 8: PES around minimum O of models 1 to 3 and wave functions of the first four vibrational states of the isolated HH system.

From top to bottom, the energy of vibrational states is increasing.

Appendix C

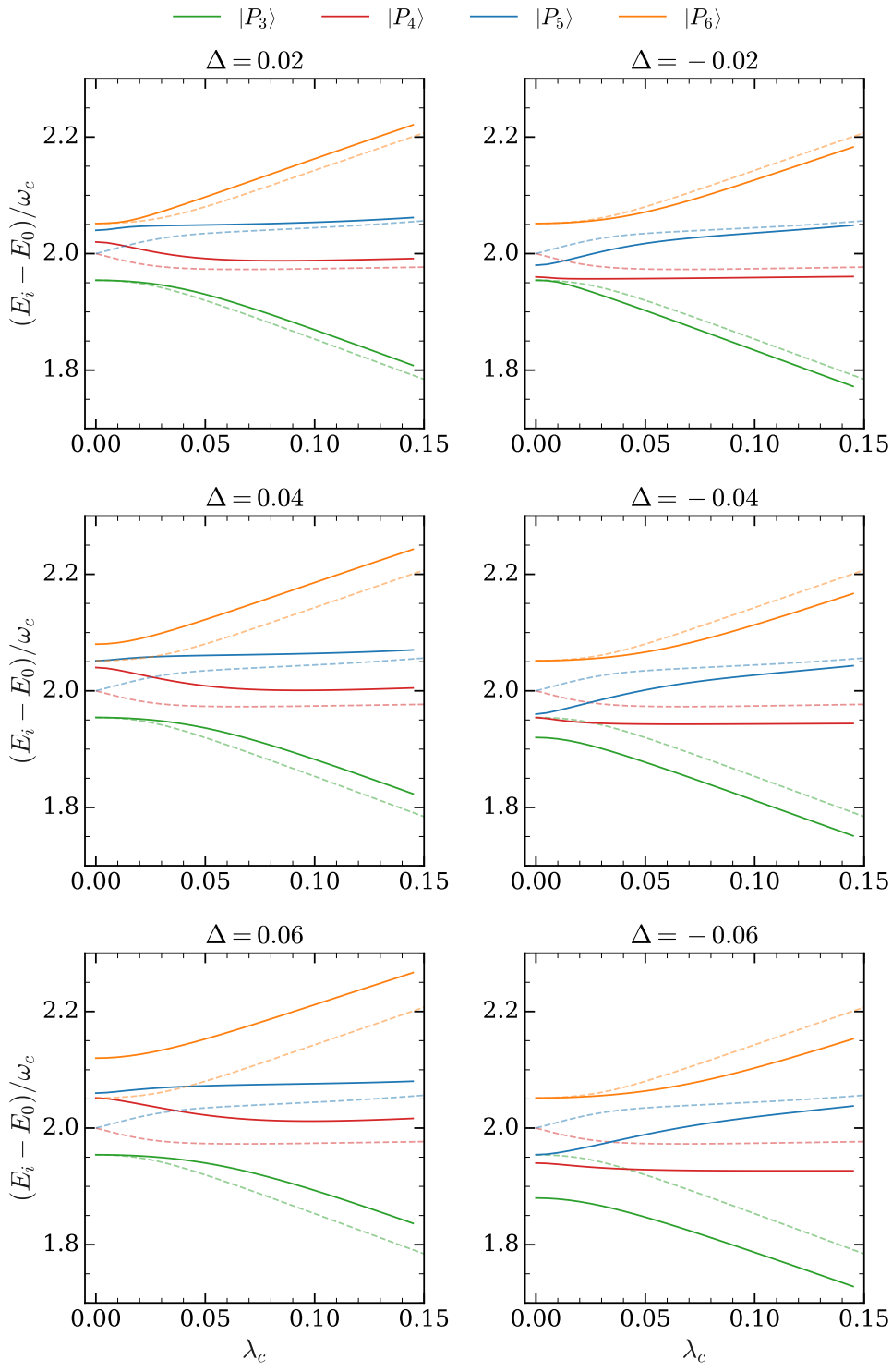

Figure 9: Cavity frequency shift of Δ relative to the first excited level for $|\Delta| = 0.02, 0.04$ and 0.06. Solid lines show energies in the case with shift Δ; energies of the case without shift in dotted lines. Energy order inversions occur in these figures, $|P_3\rangle$ at $\Delta = -0.02$ ($|P_3\rangle = |0,(2,0)'\rangle$ is not the same state for $\Delta = -0.06$ where $|P_3\rangle = |2,0,0\rangle$. A similar remark for $\Delta > 0$ with inversion between $|P_4\rangle$ and $|P_6\rangle$ is observable.

Bibliography

[1] J. George, A. Shalabney, J. A. Hutchison, C. Genet, and T. W. Ebbesen, "Liquid-Phase Vibrational Strong Coupling.," *The journal of physical chemistry letters*, pp. 1027–1031, 2015, [Online]. Available: https://api.semanticscholar.org/CorpusID:206658857

[2] L. Attal, F. Calvo, C. Falvo, and P. Parneix, "Coherent state switching using vibrational polaritons in an asymmetric double-well potential," *Phys. Chem. Chem. Phys.*, vol. 26, no. 9, pp. 7534–7544, 2024, doi: 10.1039/D3CP05568J.

[3] L. Attal, F. Calvo, C. Falvo, and P. Parneix, "Out-of-equilibrium dynamics of polaritonic states in a a 2D Hénon-Heiles system (non publié en date du rendu)," 2024.

[4] J. Zúñiga, A. Bastida, and A. Requena, "Quantum treatment of Hénon–Heiles systems using oblique coordinates," *Journal of Physics B: Atomic, Molecular and Optical Physics*, vol. 50, no. 2, p. 25101, Dec. 2016, doi: 10.1088/1361-6455/aa5082.

[5] J. Zúñiga, A. Bastida, and A. Requena, "Quantum Dynamics of Oblique Vibrational States in the Hénon–Heiles System," *The Journal of Physical Chemistry A*, vol. 127, no. 41, pp. 8663–8675, 2023, doi: 10.1021/acs.jpca.3c03122.

[6] D. T. Colbert and W. H. Miller, "A novel discrete variable representation for quantum mechanical reactive scattering via the S-matrix Kohn method," *The Journal of Chemical Physics*, vol. 96, no. 3, pp. 1982–1991, 1992, doi: 10.1063/1.462100.

[7] G. Van Rossum and F. L. Drake, *Python 3 Reference Manual*. Scotts Valley, CA: CreateSpace, 2009.

[8] J. D. Hunter, "Matplotlib: A 2D graphics environment," *Computing in Science & Engineering*, vol. 9, no. 3, pp. 90–95, 2007, doi: 10.1109/MCSE.2007.55.

[9] M. Curcic *et al.*, "Toward Modern Fortran Tooling and a Thriving Developer Community," *CoRR*, 2021, [Online]. Available: https://arxiv.org/abs/2109.07382